DOI: 10.1002/ejic.201001263

$\{Rh(P\mathit{i}Bu_3)_2\}^+$ Fragments Ligated to Arenes: From Benzene to Polyaromatic Hydrocarbons, Part I[‡] – An Experimental Approach

Anthony Woolf,[a] Adrian B. Chaplin,[a] John E. McGrady,[a] Muhsen A. M. Alibadi,[a] Nicholas Rees,[a] Sylvia Draper,[b] Frances Murphy,[b] and Andrew S. Weller*[a]

Keywords: Rhodium / Arenes / Arene ligands / Pi interactions / Hydrocarbons / Polyaromatic hydrocarbons

We report the synthesis, structural characterisation and solution-phase dynamics of a series of polyaromatic hydrocarbon complexes of the 12-electron $\{Rh(P\mathit{i}Bu_3)_2\}^+$ fragment. Crystal structures of this fragment with benzene, naphthalene, anthracene, pyrene, triphenylene and coronene are described, alongside their solution NMR spectroscopic data. The ligands map out a systematic increase in size of the aromatic subunit, and represent an approach to the limiting case of coordination to a graphene surface. The solid-state and solution structures of a $\{Rh(COD)\}^+$ fragment coordinated to a hexa-*peri*-hexabenzocoronene are also reported.

Introduction

The π coordination chemistry of transition-metal fragments with simple arenes is now a well developed area,[1–3] dating back to the first rational synthesis of $Cr(\eta^6\text{-}C_6H_6)_2$ in 1955.[4] Coordination complexes of simple fused aromatics, also called polycyclic aromatic hydrocarbons (PAH), such as naphthalene (**L3**, Scheme 1) and anthracene (**L4**) are also common.[2,5,6–10] Examples with larger PAH systems, for example triphenylene (**L5**),[10,11,12–14] and pyrene (**L6**),[10,12,13,15] are less well represented in the literature. Only one crystallographically characterized d-block complex of coronene (**L7**) has been reported.[16] Coordination to even larger PAH molecules including corannulene ($C_{20}H_{10}$), the curved carbon fragment of buckminsterfullerene,[17–19] and the C_{42} PAH hexa-*peri*-hexabenzocoronene (HBC, **L8**[20]) is also known.[21,22] Related functionalized HBC analogues in which a metal coordinates to a peripheral Lewis base incorporated into the PAH have been reported.[23] PAHs and their metal complexes (e.g. of iron) have been proposed as the source of the aromatic infrared bands observed in many astronomical objects and could be important intermediates in the formation of small molecules in interstellar space. This observation has motivated a number of gas-phase studies on metal ion ligation to extended π-systems.[24] The incorporation of transition metal centers onto the surface of PAH systems can moderate their reactivity,[25] as well as the photophysical[26] and electronic[19] properties of the hydrocarbon moiety. Transition metal functionalized PAHs also represent important models[27] for the coordination of metals to graphene and other extended carbon surfaces.[28]

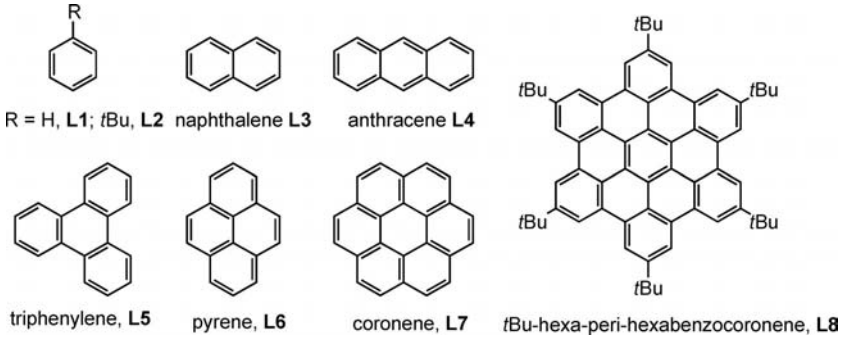

Scheme 1.

[‡] Part II: A. Woolf, M. A. M. Alibadi, A. B. Chaplin, J. E. McGrady, A. S. Weller, *Eur. J. Inorg. Chem.* **2011**, 1626–1634 (following paper).

[a] Department of Chemistry, Inorganic Chemistry Laboratories, Oxford, OX1 3QR, UK
[b] School of Chemistry, University of Dublin, Trinity College, Dublin, D2, Ireland
E-mail: andrew.weller@chem.ox.ac.uk

Supporting information for this article is available on the WWW under http://dx.doi.org/10.1002/ejic.201001263.

© 2011 Wiley-VCH Verlag GmbH & Co. KGaA, Weinheim

Transition metals coordinated to arenes can adopt a range of hapticities from η^6 through to η^1 depending on the electronic requirements of both the metal and ligand.[2] Thus the adoption of stable 18- and 16-electron configurations on one hand and the retention of maximal aromatic stabilization in the ligand on the other provide important, and potentially conflicting, driving forces for the adoption of a particular structure. In polycyclic aromatic systems haptotropic rearrangements where the metal moves from one aromatic ring to another[8,18,29] can also occur. The migration pathways in these reactions presumably reflect the best compromise where disruptions to the electronic environments of metal and ligand are minimized.

We have recently reported the synthesis of a formally 12-electron rhodium(I) complex $[Rh(P\textit{i}Bu_3)_2][BAr^F{}_4]$ [Ar^F = $C_6H_3(CF_3)_2$] that reacts with arenes, even weakly binding fluorinated ones such as C_6H_5F[30] and 1,2-$C_6H_4F_2$,[31] to give the associated π-coordination complexes, e.g. $[Rh(C_6H_5F)(P\textit{i}Bu_3)_2][BAr^F{}_4]$ (**1**) (Scheme 2). With chloro- and bromo-substituted arenes C–X activation occurs via an η-bound intermediate.[30,32] No C–H activation of the arene has been observed, in contrast to the chemistry of the related $\{Rh(\eta^5\text{-}C_5Me_5)(PMe_3)\}$ systems.[10] Given that **1** is a readily available synthon and reacts cleanly with simple arenes by the straightforward substitution of a weakly bound fluorobenzene ligand we reasoned that this would be an ideal precursor for the formation of rhodium complexes of a range of aromatic ligands of increasing size.

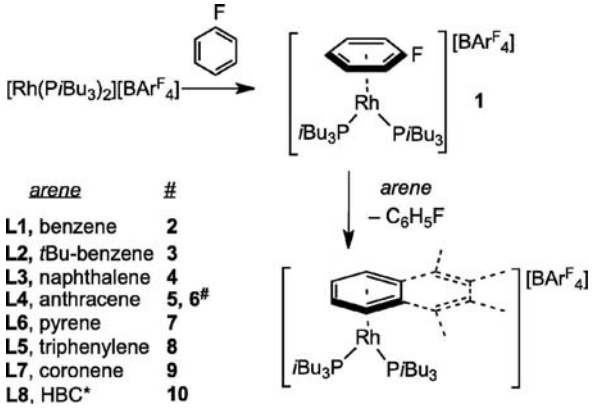

arene	#
L1, benzene	2
L2, *t*Bu-benzene	3
L3, naphthalene	4
L4, anthracene	5, 6#
L6, pyrene	7
L5, triphenylene	8
L7, coronene	9
L8, HBC*	10

Scheme 2. General synthetic scheme (# dimeric species, * with the $\{Rh(COD)\}^+$ fragment).

In this contribution we report the synthesis of complexes of the $\{Rh(P\textit{i}Bu_3)_2\}^+$ fragment with various arenes ranging from benzene to coronene (**L1**–**L7**, Scheme 2). These are characterized in the solid state and using solution-phase NMR spectroscopy. This synthetic methodology is similar to that recently reported for metal complexes of corannulene ($C_{20}H_{10}$), e.g. $[Rh(COE)_2(corannulene)][PF_6]$.[18] In addition, a solid-state structure for a $\{Rh(COD)\}^+$ (COD = 1,5-cyclooctadiene) fragment bound to HBC (**L8**) is reported. In Part II (following paper) we describe a computational investigation of these species that provides a detailed insight into the binding and motion of $\{Rh(PR_3)_2\}^+$ fragments across increasingly extended carbon surfaces.

Results and Discussion

Synthesis and Solid-State and Solution Structures

The majority of the new complexes reported here have been synthesized by the same procedure: combination of **1** with the appropriate arene (**L1** to **L7**, 5 equiv.) in CH_2Cl_2 solution. Recrystallisation from CH_2Cl_2/pentane afforded crystalline material that was initially characterised by NMR spectroscopy. Ligand **L8** required a different metal fragment, $\{Rh(COD)\}^+$. Apart from one case (anthracene, vide infra), solution NMR spectroscopic data for the complexes prepared in situ were the same as for the isolated crystalline material. For larger PAH systems (**L6** and **L7**) decomposition in solution occurred on removal of excess arene and so NMR spectroscopic data for these species were recorded from rapidly prepared crystalline samples at sub-ambient temperatures. Analysis by ESI-MS did not give the parent ion or indeed any useful information. However, analytical data on crystalline material demonstrates purity. In the following sections we discuss how the structural features of the complexes evolve as the PAH framework is extended.

Benzene and *tert*-Butylbenzene

The new compounds $[Rh(P\textit{i}Bu_3)_2(benzene)][BAr^F{}_4]$ (**2**) and $[Rh(P\textit{i}Bu_3)_2(\textit{t}Bu\text{-}benzene)][BAr^F{}_4]$ (**3**) were isolated in good yield as red-brown crystalline materials. The solid-state structures of both have been determined. Complex **2** is disordered in both the arene and $P\textit{i}Bu_3$ ligands but the disorder could be modeled satisfactorily, albeit it with the caveat that the benzene ligand was constrained to be planar in the refinement. We discuss one of these components, as the structural metrics for all are similar. The Rh–P distances in **2** are rather similar [2.2753(11) and 2.2695(12) Å], as are the Rh–C distances which range from 2.255(9)–2.430(9) Å, and are similar to those reported for $[Rh(PPh_3)_2(benzene)][BAr^F{}_4]$, 2.283(4)–2.366(4) Å.[33] The Rh–C distances in **2** fall into three, closely separated, ranges: C2/C3, 2.272(1)/2.255(9); C1/C4, 2.360(10)/2.328(8); and C5/C6, 2.414(9)/2.430(9) Å. A precise definition of the hapticity of **2** is therefore not straightforward as the distinction between bonded and non-bonded distances is not large, suggesting an η^6 (18-electron) formulation, but the pattern of Rh–C bond lengths suggests a distinct slip towards η^4 (16-electron). The Rh–C distances are comparable to those in other η^4-arene complexes of Rh^I. For example, $[Rh\{\eta^4\text{-}(C_6H_5)NHCH_2Ph\}(PPh_3)_2][PF_6]$[34] has Rh–C bonding distances spanning the range 2.288(3)–2.310(4) Å, while those assigned as non-bonding are at 2.442(3)–2.524(3) Å. The complex $[(\mu^2,\eta^1\text{:}\eta^4\text{:}\eta^1\text{-}\{1,4\text{-bis}[2\text{-(diphenylphosphanyl)ethoxy}]naphthalene\})_2Rh_2][BF_4]_2$[35] has a naphthalene ligand that is slipped to η^4, with bonding and non-bonding distances in the range 2.211(6)–2.419(6) and 2.507(6)–2.569(9) Å, respectively. $[(\eta^4\text{-}C_6H_8)Rh(PPh_3)_2][\textit{closo}\text{-}CB_{11}H_6Br_6]$ also shows similar bonded Rh–C distances [2.157(3)–2.291(3) Å].[36] As shown in Scheme 3, the plane defined by the $\{RhP_2\}$ fragment lies at an angle of

 © 2011 Wiley-VCH Verlag GmbH & Co. KGaA, Weinheim

20.2° relative to the C1–C4–Rh1 plane. The presence of a *t*Bu-group in **3** prevents the disorder of the arene ligand (although the phosphane alkyl groups are still disordered) and no constraints on the arene ring were necessary in the structural refinement. The solid-state structure of **3** shows a coordination mode similar to that of **2** although the distinction between bonded and non-bonded Rh–C distances is again not large [range 2.274(3)–2.441(3) Å]. The $\{RhP_2\}$ fragment is rotated away from the bulky *t*Bu group (twist angle 71.4°). No close π-π stacking between arenes was evident from the extended crystal structures of **2** or **3** (Figure 1).

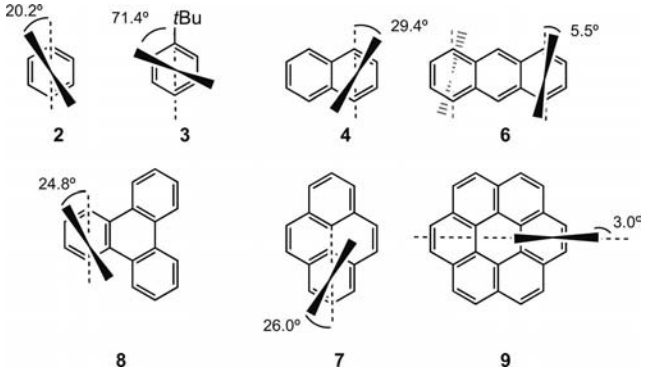

Scheme 3. Orientation of the RhP_2 fragments relative to the arene rings in the solid-state structures.

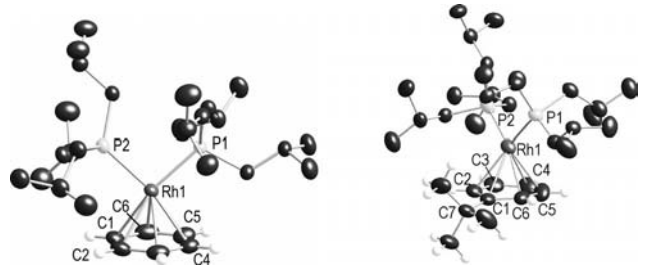

Figure 1. Solid-state structures of the cationic portion of complex **2** and **3**. Anion and hydrogen atoms on the phosphane group are not shown, nor is the minor disordered component of the alkyl phosphane groups or the benzene ligand in **2**. Thermal ellipsoids are shown at the 30% probability level. For **2**: Selected distances [Å]: Rh1–C1 2.360(10), Rh1–C2 2.272(10), Rh1–C3 2.255(9), Rh1–C4 2.328(8), Rh1–C5 2.414(9), Rh1–C6 2.430(9), Rh1–P1 2.2753(11), Rh1–P2 2.2695(12). Selected angle: P1–Rh1–P2: 95.59(4)°. For **3**: selected distances [Å]: Rh1–C1 2.441(3), Rh1–C2 2.333(3), Rh1–C3 2.274(3), Rh1–C4 2.350(4) Rh1–C5 2.441(3), Rh1–C6 2.330(4), Rh1–P1 2.274(3) Rh1–P2 2.2294(15). Selected angle: P1–Rh1–P2 97.56(6)°.

In solution at room temperature complex **2** shows a single, upfield-shifted singlet resonance in the ^1H NMR spectrum for the bound arene at δ = 6.48 (cf. free C_6H_6, δ = 7.35 ppm), consistent with coordination to a metal fragment.[1] The $^{31}P\{^1H\}$ NMR spectrum shows a single sharp doublet at δ = 25.6 [J(RhP) = 199 Hz]. In the $^{13}C\{^1H\}$ NMR spectrum the arene ligand is observed as a single environment showing coupling to ^{103}Rh, δ = 101.3 [d, J(RhC) = 2 Hz]. The observation of ^{103}Rh-^{13}C coupling suggests that arene dissociation is not occurring on the NMR timescale. A single environment is also observed for the *i*Bu methyl groups. The ^1H NMR spectrum also indicates equivalent *i*Bu groups, with a single environment for $CHMe_2$ observed as a doublet, and the CH_2CHMe_2 environment as an integral 12 H doublet of doublets [J(P,H) = 2, J(H,H) = 8 Hz]. These data are broadly similar to those reported for $[Rh(PPh_3)_2(benzene)][BAr^F_4]$[33] and $[Rh(C_6H_5F)(P\textit{i}Bu_3)_2][BAr^F_4]$.[30] The NMR spectroscopic data for **3** are similar to **2** and show equivalent *i*Bu groups. This is noteworthy as the introduction of the *t*Bu group on the arene reduces the highest possible symmetry to C_s, in which case the diastereotopic methyl groups on the *i*Bu ligands should be inequivalent in a static structure. A simple libration of the $\{Rh(P\textit{i}Bu_3)_2\}^+$ fragment would not make the methyl groups equivalent. We thus suggest that the metal fragment is rotating about the pseudo-C_6 axis of the arene ring. In support of this assignment we have recently reported examples of complexes that also show equivalent phosphorus environments in the $^{31}P\{^1H\}$ NMR spectrum, have C_s symmetry but do not undergo exchange. These show two sets of clearly-resolved *i*Bu resonances, in contrast to **3**.[32]

Naphthalene

The solid-state structure of $[Rh(P\textit{i}Bu_3)_2(naphthalene)][BAr^F_4]$ (**4**) is shown in Figure 2. The arene ligand is disordered over two closely related conformations differentiated by a slight twist of the ligand with regard to the RhP_2 plane. Only parameters for the major component (69% occupancy) are discussed. The Rh–C distances span two distinct ranges: 2.263(10)–2.405(7) (C1–C4) and 2.553(11), 2.603(8) Å (C5, C6) and the bonding is thus defined as being η^4 and the metal centre is 16-electron. The naphthalene ligand in **4** is hinged about C1–C4 [8.5(5)°] with a relatively small distortion from planarity compared to that in 18-electron $Rh(\eta^5\text{-}C_5Me_5)(\eta^4\text{-naphthalene})$ ca. 35°,[9] and $Ru(PEt_3)(\eta^4\text{-COD})(\eta^4\text{-naphthalene})$ ca. 41.5°.[6] The $\{RhP_2\}$ plane in **4** is also twisted away from the C1–C4–Rh1 plane by 29.4° (Scheme 3).

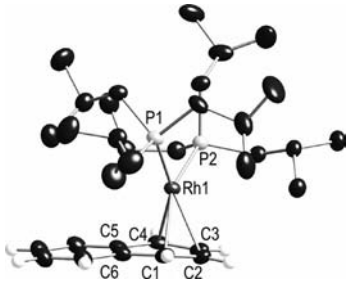

Figure 2. Solid-state structure of the cationic portion of complex **4**. See Figure 1 legend for details. Selected distances [Å]: Rh1–C1 2.405(7), Rh1–C2 2.328(7), Rh1–C3 2.243(9), Rh1–C4 2.263(10), Rh1–C5 2.553(11), Rh1–C6 2.603(8), Rh1–P1 2.3173(7), Rh1–P2 2.2485(7). Selected angles: P1–Rh1–P2 98.34(2)°.

At room temperature in solution complex **4** shows signals in the ^1H and $^{13}C\{^1H\}$ NMR spectra that are fully consistent with the arene coordination mode revealed by

 © 2011 Wiley-VCH Verlag GmbH & Co. KGaA, Weinheim

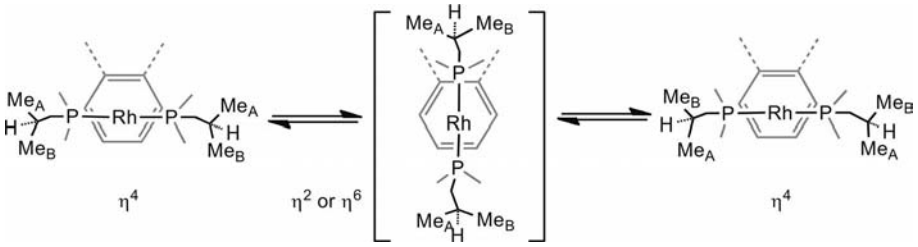

Scheme 4. Rotation of $\{RhP_2\}^+$ fragment and interchange of Me_A and Me_B. Rotation around the Rh–P bond is assumed.

the crystal structure. The symmetry of the arene is reduced to C_s and two upfield shifted aromatic resonances are observed in the ^1H NMR spectra at δ = 6.74 (2 H) and 6.03 (2 H) (for H1/4 and H2/3, respectively). Two further signals are essentially unshifted (δ = 7.54–7.46 m, 4 H) from free naphthalene (δ = 7.86 and 7.49 ppm). A single resonance (doublet) is observed in the $^{31}P\{^1H\}$ NMR spectrum at δ = 16.7 [J(RhP) = 196 Hz]. The $^{13}C\{^1H\}$ NMR spectrum also shows two upfield shifted resonances with clear coupling to ^{103}Rh, viz. δ = 96.0 [C1/4, d, J(RhC) = 3 Hz], δ = 89.5 [C2/3, d, J(RhC) = 3 Hz] and three sets of resonances in the region of free naphthalene showing no coupling to ^{103}Rh (δ = 130.3, 127.5, 125.3). These assignments, confirmed by HSQC and ^1H-^1H COSY experiments, show that decoordination of the naphthalene ring is not occurring on the NMR timescale. Crabtree has noted similar chemical shifts in [Ir(PPh_3)$_2$(2-ethylnaphthalene)][SbF_6].[37] Just as for **3**, only a single set of *i*Bu resonances is observed at room temperature, suggesting that a process that results in rotation of the $\{Rh(P\textit{i}Bu_3)_2\}^+$ fragment on the arene is relatively low energy. In principle, this could be achieved by a simple rotation about the butadiene fragment C1–C4 (Scheme 4), possibly involving an η^3-allyl-like transition state similar to that reported for a ring walking process in [Ni($R_2PCH_2CH_2PR_2$)(η^2-arene)] systems.[38] It is interesting to note that Ru(PMe_2Ph)$_3$(η^4-naphthalene),[39] which has an 18-electron configuration at the metal centre, has a strongly hinged structure and is static on the NMR timescale.

Anthracene

Mixing **1** with 5 equiv. of anthracene in CH_2Cl_2 solution immediately gave a blood-red solution assigned to a 1:1 complex [Rh(P*i*Bu$_3$)$_2$(anthracene)][BAr^F_4], **5**. NMR spectra measured immediately after mixing show a characteristic 2:2:2:2:2 pattern of resonances between δ = 7.89 and 6.04 in the aromatic region, with two higher-field resonances assigned to the coordinated portion of the arene (δ = 6.52, 6.04, 2H each). The $^{31}P\{^1H\}$ NMR spectrum shows a sharp doublet at δ = 13.6 [J(RhP) = 191 Hz]. These data are consistent with time-averaged C_s symmetry, and a structure in solution similar to **4**. After 5 min, however, complex **6**, a 2:1 adduct [Rh(P*i*Bu$_3$)$_2$(anthracene)$_2$][BAr^F_4]$_2$, starts to precipitate as dark blue crystals in high yield (based on Rh). Addition of a larger excess of anthracene failed to prevent the formation of **6**. Of all the complexes reported here, **6** is the only bis adduct observed. The data summarized above suggest a process as outlined in Scheme 5. We suggest the preferential formation of **6** over **5** is determined by the relative solubilities of monocationic **5** vs. dicationic **6**, which drives this equlibrium in favour of **6** under the reaction conditions.

Complex **6** crystallizes with crystallographically imposed centrosymmetry, with the metal fragments arranged *anti* to one another (Figure 3). Each $\{Rh(P\textit{i}Bu_3)_2\}^+$ fragment has four short Rh–C distances [2.203(4)–2.310(3) Å, Rh–C2 and Rh–C3 being the shortest] and the anthracene ligand is hinged around C1/C4 by 12.6(1)°, a somewhat larger angle than in **4**, leading to non-bonded distances to C5 and C6 of 2.704(4) and 2.708(4) Å [compared to 2.553(11), 2.603(8) Å in **4**]. We characterize the coordination mode here as being η^4-, similar to **4** and Mo(PMe_3)$_3$(anthracene).[7] As expected for a structure with metals coordinated to both faces of the PAH, there is no π-π stacking in the solid state. The Rh–P distances are the same within error, 2.3096(9) and 2.3069(9) Å. There are only a few other crystallographically characterized examples where two metals coordinate to anthracene.[13,40,41] A closely related example where two metal fragments coordinate to phenazine also adopts an *anti* arrangement.[41]

^1H and $^{31}P\{^1H\}$ NMR spectra of **6** in dilute CD_2Cl_2 (obtained by dissolving isolated crystals in excess solvent, a procedure that was necessary as **6** is sparingly soluble), show the presence of both **5** and **6**. The spectrum of **6** shows only three resonances in the aromatic region, consistent with the higher symmetry of the bis adduct (C_{2v}). These are in the ratio 2:4:4, with the most downfield signal (H7) a

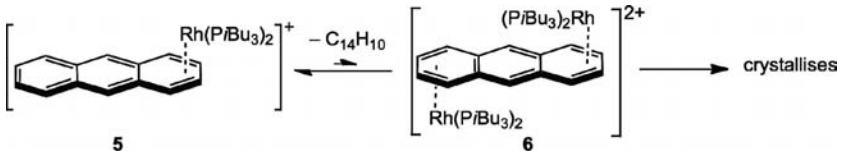

Scheme 5.

 © 2011 Wiley-VCH Verlag GmbH & Co. KGaA, Weinheim

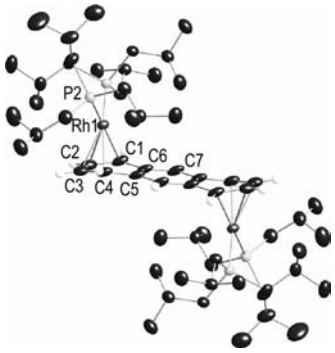

Figure 3. Solid-state structure of the dicationic portion of complex **6**. See Figure 1 legend for details. Selected distances [Å]: Rh1–C1 2.310(3), Rh1–C2 2.204(3), Rh1–C3 2.203(4), Rh1–C4 2.303(3), Rh1–C5 2.704(3), Rh1–C6 2.708(4), Rh1–P1 2.3096(9), Rh1–P2 2.3069(9). Selected angle: P1–Rh1–P2 96.57(3)°.

singlet (δ = 7.34 ppm) and the two integral 4 H signals shifted upfield (δ = 6.65, H2/3; δ = 5.76, H1/4), typical for metal coordination. After 1 h at room temperature complex **5** was the dominant species in solution (ca. 95%). The liberated $[Rh(P\textit{i}Bu_3)_2]^+$ is not observed and we presume it decomposes under the reaction conditions. This mixture is not stable and after 24 h partial decomposition of the organometallic compounds to give free anthracene is observed.

Pyrene

The solid-state structure of $[Rh(P\textit{i}Bu_3)_2(pyrene)][BAr^F{}_4]$ **7** is shown in Figure 4. The pyrene ring in **7** is planar, with a r.m.s. deviation of 0.02 Å^2. The extended structure (Figure 5) shows close π-π stacking with a distance between arenes of 3.40(4) Å, similar to the interlayer distance of 3.35 Å in graphite. There are two independent molecules in the unit cell that differ only in the degree of twist of the $\{Rh(PR_3)_2\}^+$ fragment. In other respects the bond lengths and angles in the two units are very similar, and only one set is discussed. The Rh–C(arene) distances fall into three distinct ranges, Rh–C1 and Rh–C2 being the shortest [2.255(3), 2.285(3) Å], Rh–C3 intermediate [2.404(3) Å] and Rh–C4–Rh–C6 spanning the range 2.532(3) Å (C6)–2.643(3) Å (C5). The metal fragment is orientated such that one phosphane sits over the PAH ring and the other off the side, twisted by 26.6° relative to the C2–C5–Rh1 plane. The two short Rh–C distances suggest an η^2-coordination mode,[10] giving a formal 14-electron count to the metal centre. However, if the relatively short Rh–C3 distance is also viewed as bonding then the ligand adopts an η^3-allyl-like structure, giving a 16-electron count at the metal centre and some degree of charge separation in the aromatic ligand. Both η^2- and η^3-coordination modes have precedent in Rh^I complexes. For example $(C_5Me_5)Rh(PMe_3)$(phenanthrene) is η^2,[10] while $\{LMeRh\}_2$(mesitylene) is η^3 (L = 2,6-$C_6H_3Me_2$)NC(Me)CHC(Me)N(2,6-$C_6H_3Me_2$).[42] Interestingly, this latter complex has been proposed as a model for the transition state in the fluxional pathway for movement of the metal from chemically equivalent η^4 to η^4 coordination modes. NMR data (vide infra) indicate C_s symmetry for this coordination motif, suggesting either that a truly symmetric η^3 geometry is the equilibrium structure in solution or that interconversion of two equivalent η^2 structures occurs on the NMR timescale. A closely-related complex $[Ir(\eta^5\text{-}C_5Me_5)(pyrene)][BF_4]_2$ has been assigned a η^6-structure and therefore an 18-electron count, with Ir–C distances in the range 2.229(4)–2.314(5).[12]

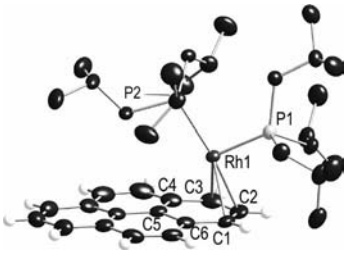

Figure 4. Solid-state structure of the cationic portion of one of the independent cations in the unit cell of complex **7**. See Figure 1 legend for details. Selected distances [Å]: Rh1–C1 2.285(3), Rh1–C2 2.255(3), Rh1–C3 2.404(3), Rh1–C4 2.586(3), Rh1–C5 2.643(3), Rh1–C6 2.532(3), Rh1–P1 2.2148(7), Rh1–P2 2.2888(6). Selected angle: P1–Rh1–P2 96.40(2)°.

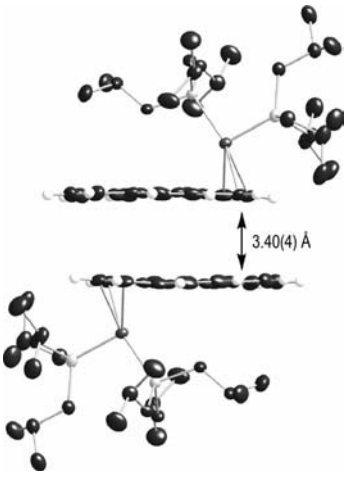

Figure 5. Packing diagram of **7** showing the interplanar separation of 3.40(4) Å.

Unlike the adducts of benzene, naphthalene, anthracene and triphenylene (vide infra) the room temperature ^{1}H NMR spectrum of **7** shows very broad signals in the arene region that contrast with the very sharp signals due to $[BAr^F{}_4]^-$ anion. The $^{31}P\{^1H\}$ NMR spectrum shows three very broad peaks in an approximate 1:4:1 ratio centred at ca. δ = 44, 22 and 13, respectively. On progressive cooling (Figure 6) to 190 K all these signals resolve into a set of sharp resonances at δ = 46.8, 21.8 and 13.5, in a similar ratio to that at room temperature. These data indicate that slowly interconverting isomeric species, **7A** and **7B**, are present (Scheme 6) over the entire temperature range. An approximate 1:0.35 ratio at 190 K equates to an energy dif-

 © 2011 Wiley-VCH Verlag GmbH & Co. KGaA, Weinheim

ference of only 0.5 kcal mol^{-1} between the two isomers. The central peak in the $^{31}P\{^1H\}$ NMR spectrum is assigned to **7A** while the outer two resonances, which also show mutual ^{31}P coupling [J(P,P) = 37 Hz], are assigned to **7B**. All three resonances show coupling to ^{103}Rh, although the magnitude of this varies: J(Rh–P) = 209 Hz **7A** (similar to the other compounds reported here) but 243 and 181 Hz for the peaks at δ = 46.8 and 13.5 respectively assigned to **7B**. In the ^1H NMR spectrum, two upfield shifted environments are observed at δ = 7.41 (t, 1 H) and δ = 6.69 (d, 2 H) for the coordinated arene in **7A**. For **7B** an upfield shifted singlet resonance (2 H) is observed for the coordinated arene at δ = 6.41. Aromatic signals between δ = 8.17 and δ = 7.62 are also observed and assigned to uncoordinated arene protons by ^1H-^1H COSY, HMQC and NOESY experiments. A $^{13}C\{^1H\}$ NMR experiment was not successful due to slow decomposition of **7** in solution.

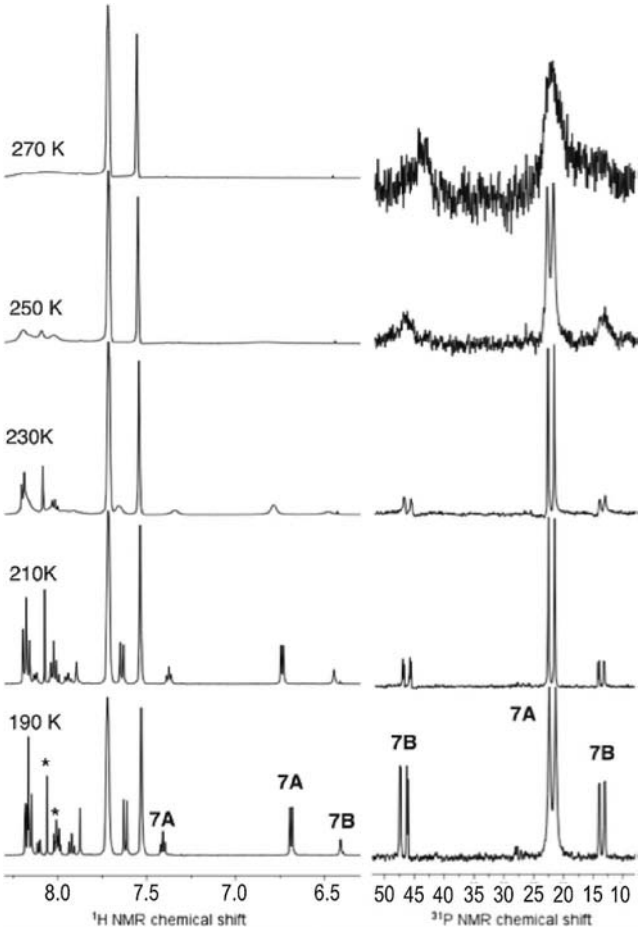

Figure 6. Variable temperature (270–190 K) ^1H and $^{31}P\{^1H\}$ NMR spectra for **7**; * indicates free pyrene.

The presence of a single ^{31}P resonance (and hence at least time-averaged C_s point symmetry) in the dominant isomer, **7A**, appears inconsistent with the solid-state structure of **7**. However, as noted above, only a relatively minor translation of the $\{Rh(PiBu_3)_2\}^+$ fragment along the C1/C2/C3 unit

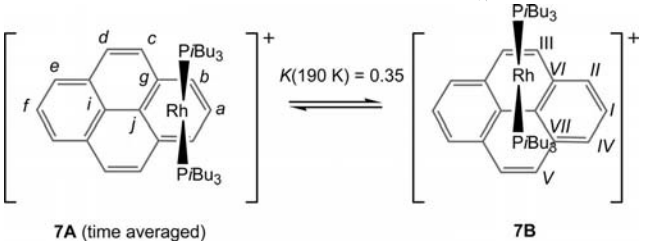

Scheme 6. Isomers **7A** and **7B**.

would result in an effective C_s-symmetric η^3-coordinated intermediate with equivalent phosphorus envrionments. **7B** also has C_s symmetry, but the observation of inequivalent phosphane environments and a single upfield-shifted singlet in the aromatic region suggest that the metal fragment is η^2-bound to C7/C8 and not undergoing rotation at this temperature. The very different J(RhP) coupling constants and chemical shifts observed for this isomer are consistent with a T-shaped coordination environment at rhodium that places one phosphane *trans* to a vacant site, very similar to the geometry observed in the solid-state structure of the coronene complex **9** (vide infra).

Upon warming the separate signals assigned to **7A** and **7B** in the ^1H NMR spectrum broaden and coalesce at 250 K. Simulation of this process afforded rate constants for exchange, for which an Eyring analysis (supporting materials) over the temperature range 220–250 K gave the activation parameters: $\Delta H^{\ddagger}$ = (11.1 ± 0.8) kcal/mol and $\Delta S^{\ddagger}$ = (–1.3 ± 1) kcal/mol/K; corresponding to an activation free energy of $\Delta G(298)^{\ddagger}$ = (11.5 ± 1) kcal/mol. Sharp peaks due to trace free pyrene are observed up to 230 K showing that rapid intermolecular exchange is not occurring at this temperature. At room temperature these peaks have broadened significantly. This available experimental data suggests that the two possible mechanisms for the isomerisation are occurring: an intramolecular haptotropic shift at lower temperatures and an additional intermolecular process where the bound-ligand exchanges with free pyrene at higher temperatures. The computed barrier for the intramolecular process (see Part II, following paper in this issue) is 11.7 kcal/mol, and the close to zero activation entropy, offers strong support that the first of the two possibilities is operating at low temperature. That intermolecular exchange is also possible at room temperature, is show by addition of d_{10}-pyrene (1 equiv.) to a CD_2Cl_2 solution of **7** that results in the formation of free protio-pyrene while the $\{Rh(PiBu_3)_2\}^+$ remains coordinated to the arene (by $^{31}P\{^1H\}$ NMR). The suggested equilibrium (at 298 K) between **5** and **6** (vide supra) also suggests an intermolecular process can operate at room temperature.

Triphenylene

The structure of $[Rh(PiBu_3)_2(triphenylene)][BAr^F_4]$ **8** is shown in Figure 7. The bond lengths clearly indicate an η^4-binding mode, with four relatively close contacts, 2.252(3)–

 © 2011 Wiley-VCH Verlag GmbH & Co. KGaA, Weinheim

2.346(3) Å, and two significantly longer (C1/C6 2.540(4) and 2.535(4) Å, respectively). This gives the metal centre a 16-electron count. There is a slight hinging about the C2–C5 axis (7.3°). The geometry of the $\{Rh(PiBu_3)_2\}^+$ fragment is similar to that observed for anthracene and naphthalene, with the RhP_2 plane rotated away from C2–C5–Rh1 plane by 24.8°. We note that [M(triphenylene)(Cp*)][BF_4] (M = Rh, Ir)[12] and $Cr(CO)_3(\eta^6$-triphenylene)[14] have been assigned as η^6-structures, although the M–C bond lengths show very similar trends to those of **8** (viz. four short and two marginally longer). The extended structure shows close π-π stacking with an average distance between arenes of 3.3(1) Å.

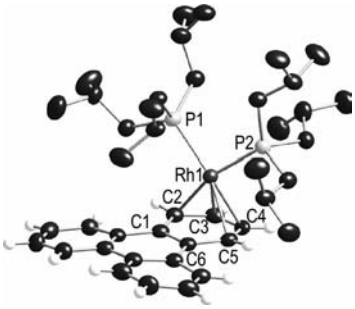

Figure 7. Solid-state structure of the cationic portion of complex **8**. See Figure 1 legend for details. Selected distances [Å]: Rh1–C1 2.540(4), Rh1–C2 2.346(3), Rh1–C3 2.312(3), Rh1–C4 2.252(3), Rh1–C5 2.286(3), Rh1–C6 2.535(3), Rh1–P1 2.2927(9), Rh1–P2 2.2603(9). Selected angle: P1–Rh1–P2 95.13(3)°.

The solution NMR spectroscopic data for complex **8** show that the metal fragment remains coordinated to one of the triphenylene rings in solution. Thus two, upfield-shifted, multiplets (2H) are observed at δ = 7.16 and 6.86 and are assigned to the aromatic ring coordinated to the $\{Rh(PiBu_3)_2\}^+$ fragment. The remaining signals observed between δ = 8.73 and 7.77, in the ratio 2:2:2:2, are essentially unshifted from free triphenylene (δ = 8.64 and 7.64 in $CDCl_3$). In the crystal structure the arene in **8** is not rigorously planar, with the two rings furthest away from the metal puckered slightly such that they become inequivalent. The fact that these rings also become equivalent on the NMR timescale suggests that this distortion is not energetically significant. The $^{31}P\{^1H\}$ NMR spectrum displays a single environment at δ = 18.7 [J(RhP) = 200 Hz]. In the $^{13}C\{^1H\}$ NMR spectrum ^{103}Rh coupling is observed for only two ^{13}C environments, δ = 99.1 [d, J(RhC) = 3 Hz] and δ = 86.4 [d, J(RhC) = 3 Hz]. A single environment observed for the *i*Bu methyl groups in both the room temperature ^1H and $^{13}C\{^1H\}$ NMR spectra, consistent with a rapid rotation of the metal fragment on the coordinated arene, as noted for **3** and **4**.

Coronene

The structure of [$Rh(PiBu_3)_2$(coronene)][BAr^F_4] **9** is shown in Figure 8.

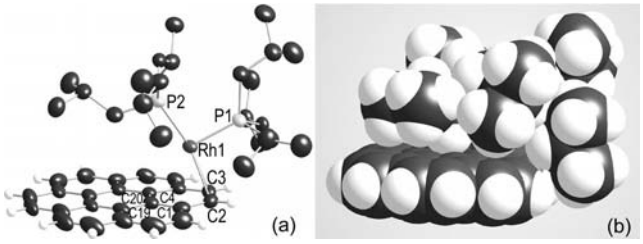

Figure 8. (a) Side and (b) space-fill (van der Waals radii) of **9**. Hydrogen atoms on the phosphane and the [BAr^F_4]$^-$ anion are omitted. Thermal ellipsoids are shown that the 30% probability level. See Figure 1 legend for details. Selected distances [Å]: Rh1–C2 2.247(4), Rh1–C3 2.247(4), Rh1–C1 2.535(4), Rh1–C4 2.523(4), Rh1–C19 2.688(4), Rh1–C20 2.682(3), Rh1–P1 2.249(3), Rh1–P2 2.296(5). Selected angles: P1–Rh1–P2 99.5(2)°.

Complex **9** crystallises with a slightly disordered RhP_2 fragment, with the phosphanes occupying two closely related sites. The Rh-arene interactions, in contrast, are not disordered. Only one set of metrics is discussed here. Rather like complex **7** the metal fragment appears to adopt an η^2-coordination mode (14-electron at metal) in the solid-state, but in this case the bonding is more clear-cut with two distances, 2.247(4)/2.247(4) Å (to C2/C3), considerably shorter that the rest [2.535(4)/2.523(4) Å for Rh–C1 and Rh–C4 and 2.688(4)/2.682(4) Å, for Rh–C19 and Rh–C20, respectively]. The Rh centre adopts a pseudo T-shaped geometry, coordinated to two phosphanes and an alkene (C2/C3). This orientation of the metal fragment places one phosphane over the arene ring-system (P2) and one off the side (P1), giving the molecule approximate C_s symmetry. A very slight hinging about the C1–C4 axis (2.3°) displaces C2 and C3 above the plane of the rest of the ligand, which is essentially planar (sum of least-squares: 0.04 Å^2). The cations pack graphitically (Bernal stacking) in the extended lattice, Figure 9, with an average interlayer separation of 3.39(4) Å. As far as we are aware complex **9** is the first transition metal complex of coronene that has been crystallographically characterized, although Ag^I[16] and Cu^I[43] complexes have been reported, both of which show η^2-metal–ligand interactions in the solid-state.

Attempts to measure NMR spectra for complex **9** at room temperature were frustrated by decomposition in the absence of excess arene ligand. To attenuate this problem a sample in CD_2Cl_2 was frozen (liquid N_2) and placed in a pre-cooled spectrometer at 190 K. On warming to 210 K decomposition starts to occur rapidly and free coronene (δ = 8.8 ppm) appears in the spectrum. At 190 K five distinct resonances are observed for the arene in the ^1H NMR spectrum, in the ratio 4:2:2:2:2. The highest-field resonance (2H) is shifted considerably from the others (δ = 6.4 vs. 8.50–7.81 ppm) indicating that the η^2-coordination observed in the solid-state persists in solution. The $^{31}P\{^1H\}$ NMR spectrum at 190 K shows two sets of resonances (doublets of doublets) in a 1:1 ratio, very similar to those assigned to the pyrene complex **7B** at 190 K: δ = 45.2 [J(RhP) 237, J(P,P) = 36 Hz], δ = 13.0 [J(RhP) = 191, J(P,P) = 36 Hz]. These data suggest that the metal fragment lies

 © 2011 Wiley-VCH Verlag GmbH & Co. KGaA, Weinheim

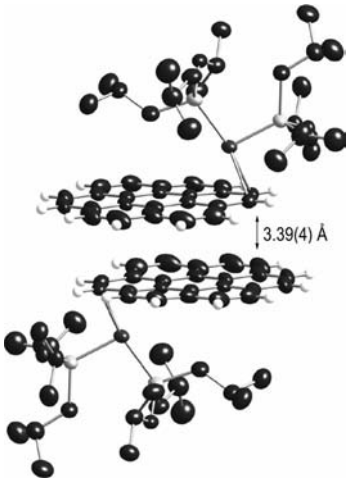

Figure 9. Packing diagram of **9** showing the interplanar separation of 3.39(4) Å.

on a reflection plane with the phosphanes asymmetrically disposed, as observed in the solid-state structure. Further support for this solution structure comes from inspection of the *i*Bu region of the low-temperature ^{1}H NMR spectrum, which shows two sets of distinct environments. A broad set of multiple resonances between δ = 2.1–0.3 that integrates to 48 H is partnered with a broad signal centered at δ = –0.55 ppm that integrates to 6 H. We assign this upfield shifted peak to a set of methyl groups from one *i*Bu ligand sitting directly over the surface of the arene ring and experiencing ring-current effects.[44] Due to decomposition at temperatures much above 200 K, we were unable to establish whether fluxional processes analogous to those occurring in the pyrene complex are accessible close to room temperature.

HBC

Addition of **1** to HBC in CH_2Cl_2 solution did not result in a reaction, with separate metal and ligand (HBC) fragments observed in solution. Reasoning that the bulky HBC ligand might bind very weakly, and therefore be unable to displace the fluorobenzene ligand in **1**, we also tried the arene-free synthon [Rh(P*i*Bu$_3$)$_2$][BAr$^F_4$],[30] but without success. However, the less sterically demanding {Rh(COD)}$^+$ fragment does bind to HBC: addition of 0.5 equiv. of [Rh(COD)Cl]$_2$/Na[BAr$^F_4$] to HBC in CH_2Cl_2 solution resulted in the formation of a new complex [Rh(COD)(HBC)][BAr$^F_4$] (**10**), dark-brown crystals of which could be isolated in 83% yield. The solid-state structure of **10** is shown in Figure 10. Complex **10** crystallises with the {Rh(COD)}$^+$ fragment disordered equally over two chemically equivalent sites on the outermost, *t*Bu-substituted, arene rings, that are related by a reflection across the centre of the ligand. The metal fragment is bound η^6, with Rh–C distances spanning a narrow range 2.342(4)–2.382(4) Å. In the extended lattice (Figure 11) the {Rh(COD)}$^+$ fragments occupy mutually adjacent positions sandwiched between two HBC rings. These outward facing arene rings show relatively close π-π stacking with a distance between arenes of 3.6(1) Å. As far as we are aware there is only one other crystallographically characterized example of a metal fragment coordinated to HBC, the {Cr(CO)$_3$} complex reported by Mullen and co-workers.[22] In this example the {Cr(CO)$_3$} fragment is also coordinated to one of the outer arene rings, and there is a similar interplanar spacing of 3.59 Å.

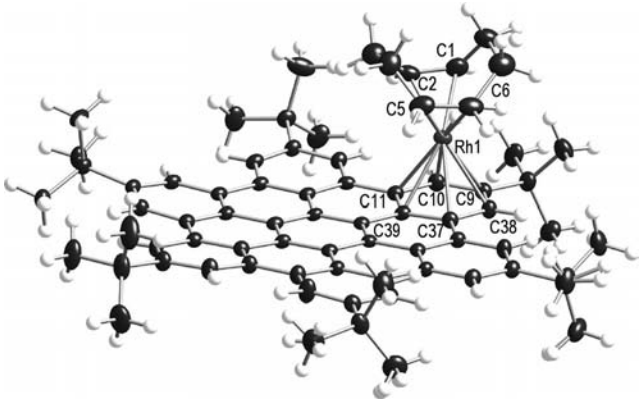

Figure 10. Solid-state structure of complex **10**. Only one of the disordered {Rh(COD)} components is shown. Hydrogen atoms and the [BAr$^F_4$]$^-$ anion are omitted. Thermal ellipsoids are shown at the 30% probability level. See Figure 1 legend for details.

Figure 11. Packing diagram of **10** showing the interplanar separation of 3.6(1) Å.

The solution NMR for **10** are consistent with the solid-state data, both indicating a C_s-symmetric structure. The ^{1}H NMR spectrum shows four *t*Bu environments in the ratio 9:9:18:18 H. Six distinct aromatic environments between δ = 9.59 and 8.06 are observed in the ratio 2:2:2:2:2:2 H. We suggest the highest field resonance is that associated with the bound metal fragment (H10/H38). Resonances due to the COD ligand are also observed. The ^{13}C{^{1}H} gives complementary information, with four *i*Bu environments and a total of 24 aromatic environments observed, four of which show coupling to ^{103}Rh. These data show that the metal is not mobile over the surface of the PAH ring on the NMR timescale.

 © 2011 Wiley-VCH Verlag GmbH & Co. KGaA, Weinheim

Conclusions

This paper has set out a detailed experimental investigation of the $\{Rh(P\textit{i}Bu_3)_2\}^+$ fragment bound to progressively larger PAH ligands. With naphthalene, anthracene and triphenylene the metal fragment adopts an η^4-coordination mode (16-electron at metal) and is not fluxional over the surface of the ligand. For pyrene and coronene the observed hapticities are lower, η^3 and η^2, and the metal fragment is fluxional over the surface of the ligand at low temperatures, or at the very least much more weakly bound. In the following paper a computational analysis leads to a detailed pictured of the underlying factors that drive both the equilibrium structures and dynamic processes (for pyrene and coronene) occurring in these systems.

Experimental Section

General: All manipulations, unless otherwise stated, were performed under an atmosphere of argon, using standard Schlenk and glove-box techniques. Glassware was oven dried at 130 °C overnight and flamed under vacuum prior to use. CH_2Cl_2, and pentane were dried using a Grubbs type solvent purification system (M. Braun SPS-800) and degassed by successive freeze-pump-thaw cycles.[45] $[RhCl(COD)]_2$, $[Rh(P\textit{i}Bu_3)_2][BAr^F_4]$,[30] $[Rh(C_6H_5F)(P\textit{i}Bu_3)_2][BAr^F_4]$ (**1**),[30] and $Na[BAr^F_4]$[46] were prepared by literature methods. All other liquid substrates were degassed by freeze-pump-thaw cycles and stored under argon over 3 Å molecular sieves; solid substrates were used as received from supplier. CD_2Cl_2 was distilled under vacuum from CaH_2 and stored over 3 Å molecular sieves. HBC was prepared by the published procedure.[22] All other materials were purchased from commercial sources. All the new complexes discussed have been characterized in solution by NMR spectroscopy. Unless stated NMR spectra were recorded in CD_2Cl_2 solutions. Assignments were aided by ^{1}H-^{1}H COSY and HSQC experiments. NMR spectra were recorded on a Bruker AVC 500 MHz or a Varian Unity Plus 500 MHz spectrometer at 298 K unless otherwise stated. All samples, deuterated and non-deuterated, were locked and referenced to CD_2Cl_2 (1 H δ = 5.32 ppm).

General Synthetic Methodology for Compounds 2 to 9: To a Young crystallisation tube containing **1** (0.030 g, 0.021 mmol), the relevant arene ligand (0.102 mmol, 5 equiv.) and CH_2Cl_2 (3 cm^3) were added and stirred for 5 min. The solution was layered with pentane at room temperature; slow diffusion of the pentane led to crystallisation isolated product formation over 1–4 d. Crystals obtained were washed with pentane (3×10 cm^3). Yields and microanalytical data are presented in Table 1.

$[Rh(COD)(6\text{-}\textit{t}Bu\text{-}HBC)][BAr^F_4]$ (10): To a Young crystallisation tube containing $[RhCl(COD)]_2$ (0.003 g, 0.006 mmol), $Na[BAr^F_4]$ (0.030 g, 0.021 mmol, 2.2 equiv.) and 6-*t*Bu-HBC (0.010 g, 0.012 mmol, 2 equiv.) CH_2Cl_2 (3 cm^3) was added and stirred for 5 min. The solution was layered with pentane at room temperature; slow diffusion of the pentane led to isolated product crystal formation over 48 h. Crystals obtained were washed with pentane (3×10 cm^3).

$[Rh(benzene)(P\textit{i}Bu_3)_2][BAr^F_4]$ (2): ^{1}H NMR (CD_2Cl_2, 500 MHz, 290 K): δ = 7.72 (br., 8 H, BAr^F_4), 7.56 (s, 4 H, BAr^F_4), 6.48 (s, 6 H, H^{Ar}), 2.00–1.89 (m, 6 H, PCH_2CH), 1.56 (dd, J_{HH} = 8, J_{HP} = 2 Hz, 12 H, CH_2), 1.08 (d, J_{HH} = 7 Hz, 36 H, Me) ppm. $^{31}P\{^1H\}$ NMR (CD_2Cl_2, 121 MHz, 290 K): δ = 25.6 (d, $^1J_{RhP}$ = 198 Hz) ppm. $^{13}C\{^1H\}$ NMR (CD_2Cl_2, 126 MHz, 290 K): δ = 162.31 (q, $^1J_{BC}$ = 50 Hz, BAr^F_4), 135.36 (s, BAr^F_4), 129.43 (qq, $^2J_{FC}$ = 32, $^4J_{BC}$ = 3 Hz, BAr^F_4), 125.16 (q, $^1J_{FC}$ = 272 Hz, BAr^F_4), 118.14–117.93 (m, BAr^F_4), 101.31 (d, $^1J_{RhC}$ = 2 Hz, C^{Ar}), 39.96–39.81 (m, CH_2), 26.89 (s, Me), 25.64–25.58 (m, PCH_2CH) ppm.

$[Rh(\textit{tert}\text{-}butylbenzene)(P\textit{i}Bu_3)_2][BAr^F_4]$ (3): ^{1}H NMR (CD_2Cl_2, 500 MHz, 290 K): δ = 7.72 (br., 8 H, BAr^F_4), 7.56 (s, 4 H, BAr^F_4), 7.23 (t, J_{HH} = 6 Hz, 1 H, H^4), 6.18 (d, J_{HH} = 6 Hz, 2 H, H^2), 5.92 (t, J_{HH} = 6 Hz, 2 H, H^3), 1.98 (m, 6 H, PCH_2CH), 1.58 (dd, J_{HH} = 6, $^1J_{HP}$ = 2 Hz, 12 H, CH_2), 1.38 (s, 9 H, *t*Bu), 1.07 (d, J_{HH} = 7 Hz, 36 H, Me_2) ppm. $^{31}P\{^1H\}$ NMR (CD_2Cl_2, 121 MHz, 290 K): δ = 26.1 (d, J_{RhP} = 203 Hz) ppm. $^{13}C\{^1H\}$ NMR (CD_2Cl_2, 126 MHz, 290 K): δ = 162.32 (q, J_{BC} = 50 Hz, BAr^F_4), 142.08 (s, C^1), 135.36 (s, BAr^F_4), 129.42 (qq, J_{FC} = 32, J_{BC} = 3 Hz, BAr^F_4), 125.17 (q, J_{FC} = 272 Hz, BAr^F_4), 118.23–117.92 (m, BAr^F_4), 105.71 (s, C^4), 97.58 (s, $^1J_{RhC}$ = 2 Hz, C^2), 95.28 (s, J_{RhC} = 2 Hz, C^3), 40.22–39.91 (m, CH_2), 34.70 (s, *C*tBu), 31.38 (s, *t*Bu), 26.85–26.44 (m, Me), 25.69 (s, PCH_2CH) ppm.

$[Rh(naphthalene)(P\textit{i}Bu_3)_2][BAr^F_4]$ (4): ^{1}H NMR (CD_2Cl_2, 500 MHz, 290 K): δ = 7.72 (br., 8 H, BAr^F_4), 7.56 (s, 4 H, BAr^F_4), 7.54–7.46 (m, 4 H, H^7 and H^8), 6.76–6.72 (m, 2 H, H^1), 6.06–6.01 (m, 2 H, H^2), 1.85–1.73 (m, 6 H, PCH_2CH), 1.59 (dd, J_{HH} = 8, J_{HP} = 2 Hz, 12 H, CH_2), 1.00 (d, J_{HH} = 7 Hz, 36 H, Me) ppm. $^{31}P\{^1H\}$ NMR (CD_2Cl_2, 121 MHz, 290 K): δ = 16.7 (d, J_{RhP} = 196 Hz) ppm. $^{13}C\{^1H\}$ NMR (CD_2Cl_2, 126 MHz, 290 K): δ = 162.31 (q, J_{BC} = 50 Hz, BAr^F_4), 135.36 (s, BAr^F_4), 130.31 (s, C^7 or C^8), 129.42 (qq, J_{FC} = 31, J_{BC} = 3 Hz, BAr^F_4), 127.49 (s, C^5), 125.27 (s, C^7 or C^8), 125.16 (q, J_{FC} = 272 Hz, BAr^F_4), 118.16–117.94 (m, BAr^F_4), 96.01 (d, J_{RhC} = 3 Hz, C^1), 89.51 (d, J_{RhC} = 3 Hz, C^2), 39.06–38.80 (m, CH_2), 26.63 (s, Me), 25.54–25.26 (m, PCH_2CH) ppm.

$[Rh(anthracene)(P\textit{i}Bu_3)_2][BAr^F_4]$ (5): ^{1}H NMR (CD_2Cl_2, 500 MHz, 290 K): δ = 7.94 (s, 2 H, H^3), 7.89–7.84 (m, H^4 or H^5), 7.72 (br., 8 H, BAr^F_4), 7.61–7.58 (m, H^4 or H^5), 7.56 (s, 4 H, BAr^F_4), 6.55–6.49 (m, 4 H, H^2), 6.09–6.04 (m, 4 H, H^1), 1.81–0.85 (m, *i*Bu) ppm. $^{31}P\{^1H\}$ NMR (CD_2Cl_2, 121 MHz, 290 K): δ = 13.6 (d, $^1J_{RhP}$ = 191 Hz) ppm.

$[\{Rh(P\textit{i}Bu_3)_2\}_2(anthracene)][BAr^F_4]_2$ (6): ^{1}H NMR (CD_2Cl_2, 500 MHz, 290 K): δ = 7.72 (br., 8 H, BAr^F_4), 7.56 (s, 4 H, BAr^F_4),

Table 1. Isolated yields and analytical data for the new complexes.

Complex	Mass [mg]	Yield [%]	Crystal colour	Calcd. C, H (%)	Found C, H (%)
2	26.8	88	red-brown	52.47, 5.08	52.32, 4.84
3	23.1	73	red-brown	53.67, 5.36	53.15, 5.46
4	25.8	82	brown	52.89, 4.98	52.32, 4.84
6	49.7	81	dark-blue	54.28, 4.95	53.80, 5.30
7	26.1	79	yellow-brown	54.98, 4.87	54.13, 4.70
8	26.9	80	brown	55.58, 4.92	55.42, 4.64
9	18.6	53	dark-brown	57.50, 4.70	56.60, 5.41
10	33.7	83	dark-brown	65.84, 4.69	65.76, 4.72

 © 2011 Wiley-VCH Verlag GmbH & Co. KGaA, Weinheim

7.34 (s, 2 H, H^7), 6.68–6.63 (m, 4 H, H^1), 5.79–5.74 (m, 4 H, H^2), 1.81–0.85 (m, *i*Bu) ppm. $^{31}P\{^1H\}$ NMR (CD_2Cl_2, 121 MHz, 290 K): δ = 14.4 (d, $^1J_{RhP}$ = 190 Hz) ppm.

[Rh(pyrene)(P*i*Bu$_3$)$_2$][BAr$^F_4$] (7): ^1H NMR (CD_2Cl_2, 500 MHz, 290 K): δ = 7.9 (br., 10 H, H^{Ar}), 7.72 (br., 8 H, BAr^F_4), 7.56 (s, 4 H, BAr^F_4), 1.76 (br., 6 H, PCH_2CH), 1.36 (br., 12 H, CH_2), 0.94 (d, J_{HH} = 6 Hz, 36 H, Me) ppm. $^{31}P\{^1H\}$ NMR (CD_2Cl_2, 121 MHz, 290 K): δ = 44.2 (vbr.), 22.1 (vbr.), 13.7 (vbr.) ppm. ^1H NMR (CD_2Cl_2, 500 MHz, 190 K): δ = 8.21 (d, J_{HH} = 6.24 Hz, H_e), 8.20 (d, J_{HH} = 6.24 Hz, H_d), 8.02 (f, J_{HH} = 6.24 Hz, H_f), 7.65 (d, $^1J_{HH}$ = 9.03 Hz, H_c), 7.45 (t, J_{HH} = 6.24 Hz, H_a), 6.70 (d, J_{HH} = 6.24 Hz, H_b), 8.14 (d, J_{HH} = 7.55 Hz, H_{IV}), 8.05 (d, J_{HH} = 7.90 Hz, H_{II}), 7.95 (vt, J_{HH} = 7.9 Hz, H_I), 6.44 (s, H_{III}), 1.50 (s, 6 H, PCH_2CH), 1.20 (s, 6 H, PCH_2), 0.74 (d, J_{HH} = 7 Hz, 36 H, Me), 0.41 (s br, 6 H, PCH_2) ppm. $^{31}P\{^1H\}$ NMR (CD_2Cl_2, 121 MHz, 190 K): δ = 46.8 [dd, J_{RhP} = 243, J_{PP} = 37 Hz, P^1], 21.8 [d, J_{RhP} = 209 Hz, outer-RhP_2], 13.5 (dd, J_{RhP} = 181, J_{PP} = 37 Hz, P^2) ppm. $^{13}C\{^1H\}$ NMR (CD_2Cl_2, 500 MHz, 190 K): δ = 132.3 (C_D), 129.8 (C_H), 128.3 (C_E), 124.0 (C_C), 122.6 (C_F), 120.7 (C_J), 114.9 (Ci), 112.1 (C_G), 98.9 (C_A), 91.0 (C_B), 130.7 (C_{VII}), 127.9 (C_{II} & C_V), 127.3 (C_{IV}), 124.9 (C_I), 120.5 (C_{VI}), 117.2 (C_{VIII}), 84.4 (C_{III}). See Scheme 6 for labelling scheme.

[Rh(triphenylene)(P*i*Bu$_3$)$_2$][BAr$^F_4$] (8): ^1H NMR (CD_2Cl_2, 500 MHz, 290 K): δ = 8.73 (d, J_{HH} = 8 Hz, 2 H, H^{16}), 8.39 (d, J_{HH} = 8 Hz, 2 H, H^{17}), 7.87 (t, J_{HH} = 7 Hz, 2 H, H^{16} or H^{15}), 7.77 (t, J_{HH} = 7 Hz, 2 H, H^{16} or H^{15}), 7.72 (br., 8 H, BAr^F_4), 7.56 (s, 4 H, BAr^F_4), 7.19–7.14 (m, 2 H, H^2), 6.89–6.82 (m, 2 H, H^1),1.72–1.60 (m, 6 H, PCH_2CH), 1.48 (dd, J_{HH} = 7, J_{HP} = 2 Hz, 12 H, CH_2), 0.86 (d, J_{HH} = 7 Hz, 36 H, Me) ppm. $^{31}P\{^1H\}$ NMR (CD_2Cl_2, 121 MHz, 290 K): δ = 18.7 (d, $^1J_{RhP}$ = 200 Hz) ppm. $^{13}C\{^1H\}$

Table 2. Crystallographic data.

	2	**3**	**4**	**6**
Formula	$C_{62}H_{72}BF_{24}P_2Rh$	$C_{66}H_{80}BF_{24}P_2Rh$	$C_{66}H_{74}BF_{24}P_2Rh$	$C_{126}H_{142}B_2F_{48}P_4Rh_2$
M	1448.86	1504.96	1498.91	2919.72
T [K]	210(2)	150(2)	150(2)	150(2)
Crystal System	monoclinic	monoclinic	monoclinic	triclinic
Space group	$P2_1/n$	$P2_1/c$	$P2_1/c$	$P\bar{1}$
a [Å]	22.00140(10)	13.31840(10)	19.7734(2)	12.74970(10)
b [Å]	13.16180(10)	13.50660(10)	13.57780(10)	16.0482(2)
c [Å]	25.5819(2)	39.2845(2)	25.6956(2)	17.8161(2)
α [°]	90	90	90	75.1320(6)
β [°]	113.9717(3)	98.5126(3)	97.5578(4)	89.9429(5)
γ [°]	90	90	90	81.2896(5)
V [Å^3]	6768.99(8)	6988.89(8)	6838.80(10)	3479.93(6)
Z	4	4	4	1
Density [g cm^{-3}]	1.422	1.430	1.456	1.393
μ [mm^{-1}]	0.402	0.393	0.401	0.392
θ range [°]	$5.10 \leq \theta \leq 25.03$	$5.12 \leq \theta \leq 26.37$	$5.10 \leq \theta \leq 26.37$	$5.09 \leq \theta \leq 26.37$
Reflections collected	23091	27115	24998	24985
R_{int}	0.0185	0.0293	0.0193	0.0269
Data/restraints/parameters	11839/2326/1282	14114/1798/1235	13815/1154/1112	14093/1716/1154
*R*1 [$I > 2\sigma(I)$]	0.0587	0.0489	0.0411	0.0464
*wR*2 [all data]	0.1685	0.1319	0.1055	0.1339
GoF	1.018	1.039	1.023	1.079
Largest diff. pk and hole [e Å^{-3}]	0.729, –0.813	1.163, –1.514	0.808, –0.488	0.682, –0.574
	7	**8**	**9**	**10**
Formula	$C_{73}H_{78}BCl_2F_{24}P_2Rh$	$C_{74}H_{78}BF_{24}P_2Rh$	$C_{80}H_{78}BF_{24}P_2Rh$	$C_{106}H_{90}BF_{24}Rh$
M	1657.91	1599.02	1671.08	1933.50
T [K]	150(2)	150(2)	150(2)	150(2)
Crystal System	triclinic	orthorhombic	triclinic	triclinic
Space group	$P\bar{1}$	*Pbca*	$P\bar{1}$	$P\bar{1}$
a [Å]	20.0331(2)	18.43130(10)	14.8314(2)	13.66330(10)
b [Å]	20.1330(2)	24.51990(10)	17.7262(2)	19.4347(2)
c [Å]	21.1109(2)	32.3168(2)	18.1889(3)	21.1239(3)
α [°]	110.3310(5)	90	113.5908(6)	107.3148(5)
β [°]	105.1706(5)	90	106.7840(7)	94.1354(5)
γ [°]	100.2469(4)	90	97.4030(7)	97.9542(6)
V [Å^3]	7358.12(12)	14605.05(13)	4029.53(10)	5265.36(10)
Z	4	8	2	2
Density [g cm^{-3}]	1.497	1.454	1.377	1.220
μ [mm^{-1}]	0.451	0.381	0.348	0.247
θ range [°]	$5.13 \leq \theta \leq 26.37$	$5.10 \leq \theta \leq 26.37$	$5.12 \leq \theta \leq 25.03$	$5.13 \leq \theta \leq 26.37$
Reflections collected	50990	97799	29289	37185
R_{int}	0.0222	0.0675	0.0220	0.0279
Data/restraints/parameters	29393/1313/2180	14812/1134/1170	16326/2202/1414	21347/1795/1622
*R*1 [$I > 2\sigma(I)$]	0.0416	0.0462	0.0627	0.0901
*wR*2 [all data]	0.1136	0.1259	0.1924	0.2535
GoF	1.034	1.033	1.065	1.057
Largest diff. pk and hole [e Å^{-3}]	0.640, –0.603	0.797, –0.556	0.939, –0.680	1.695, –0.610

 © 2011 Wiley-VCH Verlag GmbH & Co. KGaA, Weinheim

NMR (CD_2Cl_2, 126 MHz, 290 K): δ = 162.31 (q, J_{BC} = 50 Hz, BAr^F_4), 135.37 (s, BAr^F_4), 131.22 (s, C^8), 130.19 (s, C^{15}), 129.42 (qq, J_{FC} = 31, J_{BC} = 3 Hz, BAr^F_4), 129.02 (s, 2 H, C^{16}), 126.00 (s, 2 H, C^{13}), 125.16 (q, J_{FC} = 272 Hz, BAr^F_4), 124.73 (s, 2 H, C^{14}), 123.95 (s, 2 H, C^{17}), 120.42 (s, 2 H, C^1), 118.23–118.09–117.90 (m, BAr^F_4), 99.07 (d, J_{RhC} = 3 Hz, 2 H, C^2), 86.37 (d, J_{RhC} = 3 Hz, 2 H, C^3), 39.03–38.64 (m, CH_2), 26.46 (s, Me), 25.50–25.11 (m, PCH_2CH) ppm.

[Rh(coronene)(P*i*Bu$_3$)$_2$][BAr$^F_4$] (9): ^{1}H NMR (CD_2Cl_2, 500 MHz, 290 K): δ = 8.52 (vbr, 12 H, H^{Ar}), 7.72 (br., 8 H, BAr^F_4), 7.56 (s, 4 H, BAr^F_4), 2.02 (br., 6 H, PCH_2CH), 1.55 (br., 12 H, CH_2), 0.58 (br., 36 H, Me) ppm. $^{31}P\{^1H\}$ NMR (CD_2Cl_2, 121 MHz, 290 K): δ = 48.4 (br.), 26.4 (br.) ppm. ^{1}H NMR (CD_2Cl_2, 500 MHz, 200 K): δ = 8.72 (obscured, H^{Ar}), 8.35 (s, 2 H, H), 8.32 (d, J_{HH} = 7 Hz, 2 H, H), 8.18–8.11 (m, 4 H, H), 7.90 (d, J_{HH} = 7 Hz, 2 H, 2 H), 7.72 (br., 8 H, BAr^F_4), 7.56 (s, 4 H, BAr^F_4), 1.86 (br.), 1.45 (br.), 0.81 (t, 6 H), –0.45 (br., 6 H, Me on P^2) ppm. $^{31}P\{^1H\}$ NMR (CD_2Cl_2, 121 MHz, 190 K): δ = 45.2 (dd, J_{RhP} = 237, J_{PP} = 36 Hz, P^1), 13.0 (dd, J_{RhP} = 191, J_{PP} = 36 Hz, P^2) ppm.

[Rh(6-*t*Bu-HBC)(COD)][BAr$^F_4$] (10): ^{1}H NMR (CD_2Cl_2, 500 MHz, 290 K): δ = 9.59 (s, 2 H, H^{Ar}), 9.48 (s, 2 H, H^{Ar}), 9.45 (s, 2 H, H^{Ar}), 9.42 (s, 2 H, H^{Ar}), 8.82 (s, 2 H, H^{Ar}), 8.06 (s, 2 H, H^1), 7.72 (br., 8 H, BAr^F_4), 7.56 (s, 4 H, BAr^F_4), 3.73 (s, 4 H, $C_4H_8C_4H_4$), 1.96 (s, 9 H, *t*Bu), 1.86 (s, 9 H, *t*Bu), 1.85 (s, 18 H, *t*Bu), 1.81 (s, 18 H, *t*Bu), 1.60 (s, 8 H, $C_4H_8C_4H_4$) ppm. $^{13}C\{^1H\}$ NMR (CD_2Cl_2, 126 MHz, 290 K): δ = 151.82 (d, J_{RhC} = 3 Hz, C^{Ar}), 151.60 (s, C^{Ar}), 135.35 (s, BAr^F_4), 132.38 (s, C^{Ar}), 131.35 (d, J_{RhC} = 4 Hz, C^{Ar}), 130.30 (s, C^{Ar}), 129.44 (qq, J_{FC} = 32, J_{BC} = 3 Hz, BAr^F_4), 125.14 (q, J_{FC} = 272 Hz, BAr^F_4), 125.02 (s, C^{Ar}), 124.82 (s, C^{Ar}), 124.23 (s, C^{Ar} coupled to H^{Ar}), 123.72 (s, C^{Ar}), 123.62 (s, C^{Ar}), 122.47 (s, C^{Ar}), 121.09 (s, C^{Ar} coupled to H^{Ar}), 120.92 (s, C^{Ar} coupled to H^{Ar}), 120.87 (s, C^{Ar}), 120.54 (s, C^{Ar} coupled to H^{Ar}), 120.38 (s, C^{Ar} coupled to H^{Ar}), 120.06 (s C^{Ar}), 118.22–117.93 (m, BAr^F_4), 115.13 (s C^{Ar}), 109.13 (s C^{Ar}), 108.87 (d, J_{RhC} = 2 Hz, C^{Ar}), 102.78 (s C^{Ar}), 91.48 (d, $^1J_{RhC}$ = 2 Hz, C^1), 83.45 (d, J_{RhC} = 13 Hz, C^2), 36.44 (t, Ct^{Bu} coupled to Ht^{Bu}), 32.19 (s, *t*Bu), 32.05 (s, *t*Bu), 31.25 (s, *t*Bu), 31.17 (s, *t*Bu) ppm.

Crystallography: Relevant details about the structure refinements are given in Table 2. Data were carried on an Enraf Nonius Kappa CCD diffractometer using graphite monochromated Mo-K_α radiation (λ = 0.71073 Å) and a low-temperature device;[47] data was collected using COLLECT, reduction and cell refinement was performed using DENZO/SCALEPACK.[48] Structures were solved using SHELXS-97 (**7**)[49] and SIR2004 (for **2**, **3**, **4**, **6**, **8**, **9**, **10**)[50] and refined full-matrix least-squares on F^2 using SHELXL-97.[49] All non-hydrogen atoms were refined anisotropically. Problematic solvent disorder in the structures of **6**, **9** and **10** was treated using the SQUEEZE algorithm.[51] Further details of disorder modelling are documented in the crystallographic information files under the heading _refine_special_details. Restraints to thermal parameters were applied were necessary in order to maintain sensible values. Graphical representations of the structures were made using CrystalMaker.

CCDC-797081 (for **2**), -797082 (for **3**), -797083 (for **4**), -797084 (for **6**), -797085 (for **7**), -797086 (for **8**), -797087 (for **9**), and -797088 (for **10**) contain the supplementary crystallographic data for this paper. These data can be obtained free of charge from The Cambridge Crystallographic Data Centre via www.ccdc.cam.ac.uk/data_request/cif.

Supporting Information (see footnote on the first page of this article): Figure S1, Experimental and simulated NMR spectroscopic data for the exchange process in **7**; Figure S2, Eyring plot and activation parameters for the exchange process in **7**.

[1] C. Elschenbroich, *Organometallics*, Wiley-VCH, Weinheim, Germany, **2006**.
[2] S. M. Hubig, S. V. Lindeman, J. K. Kochi, *Coord. Chem. Rev.* **2000**, *200*, 831–873.
[3] P. J. Fagan, M. D. Ward, J. C. Calabrese, *J. Am. Chem. Soc.* **1989**, *111*, 1698–1719; E. L. Muetterties, J. R. Bleeke, E. J. Wucherer, T. Albright, *Chem. Rev.* **1982**, *82*, 499–525.
[4] E. O. Fischer, W. Hafner, *Z. Naturforschung, Teil B* **1955**, *10*, 665–668.
[5] For leading references, see: J. Gimeno, V. Cadierno, P. Crochet, *Comprehensive Organometallic Chemistry* (Eds.: R. H. Crabtree, D. M. P. Mingos), Elsevier, New York, **2007**, vol. 6, p. 485–550; P. A. Wender, T. J. Williams, *Angew. Chem. Int. Ed.* **2002**, *41*, 4550–4551; C. R. Landis, J. Halpern, *Organometallics* **1983**, *2*, 840–842; L. Hintermann, L. Xiao, A. Labonne, U. Englert, *Organometallics* **2009**, *28*, 5739–5748.
[6] M. A. Bennett, Z. B. Lu, X. Q. Wang, M. Bown, D. C. R. Hockless, *J. Am. Chem. Soc.* **1998**, *120*, 10409–10415.
[7] G. Zhu, K. E. Janak, J. S. Figueroa, G. Parkin, *J. Am. Chem. Soc.* **2006**, *128*, 5452–5461.
[8] A. Stanger, H. Weismann, *J. Organomet. Chem.* **1996**, *515*, 183–191.
[9] J. Muller, P. E. Gaede, C. Hirsch, K. Qiao, *J. Organomet. Chem.* **1994**, *472*, 329–335.
[10] R. M. Chin, L. Z. Dong, S. B. Duckett, M. G. Partridge, W. D. Jones, R. N. Perutz, *J. Am. Chem. Soc.* **1993**, *115*, 7685–7695.
[11] For representative examples of triphenylene complexes, see: M. Munakata, G. L. Ning, Y. Suenaga, T. Kuroda-Sowa, M. Maekawa, T. Ohta, *Angew. Chem. Int. Ed.* **2000**, *39*, 4555–4556; J. Muller, C. Hirsch, K. Qiao, K. Ha, *Z. Anorg. Allg. Chem.* **1996**, *622*, 1441–1448.
[12] M. Maekawa, T. Minematsu, A. Nabei, H. Konaka, T. Kuroda-Sowa, M. Munakata, *Inorg. Chim. Acta* **2006**, *359*, 168–182.
[13] F. A. Cotton, E. V. Dikarev, M. A. Petrukhina, *J. Am. Chem. Soc.* **2001**, *123*, 11655–11663.
[14] R. D. Rogers, J. L. Atwood, T. A. Albright, W. A. Lee, M. D. Rausch, *Organometallics* **1984**, *3*, 263–270.
[15] For representative examples of pyrene complexes, see: J. A. Reingold, K. L. Virkaitis, G. B. Carpenter, S. Sun, D. A. Sweigart, P. T. Czech, K. R. Overly, *J. Am. Chem. Soc.* **2005**, *127*, 11146–11158; A. Arrais, E. Diana, G. Gervasio, R. Gobetto, D. Marabello, P. L. Stanghellini, *Eur. J. Inorg. Chem.* **2004**, 1505–1513; M. Gorlov, L. Kloo, *Coord. Chem. Rev.* **2008**, *252*, 1564–1576.
[16] M. Munakata, L. P. Wu, T. Kuroda-Sowa, M. Maekawa, Y. Suenaga, G. L. Ning, T. Kojima, *J. Am. Chem. Soc.* **1998**, *120*, 8610–8618.
[17] For representative examples of corannulene complexes, see: M. A. Petrukhina, *Angew. Chem. Int. Ed.* **2008**, *47*, 1550–1552.
[18] J. S. Siegel, K. K. Baldridge, A. Linden, R. Dorta, *J. Am. Chem. Soc.* **2006**, *128*, 10644–10645.
[19] R. J. Angelici, B. Zhu, S. Fedi, F. Laschi, P. Zanello, *Inorg. Chem.* **2007**, *46*, 10901–10906.
[20] M. D. Watson, A. Fechtenkotter, K. Mullen, *Chem. Rev.* **2001**, *101*, 1267–1300.
[21] B. El Hamaoui, L. Zhi, J. Wu, J. Li, N. T. Lucas, Z. Tomovic, U. Kolb, K. Mullen, *Adv. Funct. Mater.* **2007**, *17*, 1179–1187.
[22] P. T. Herwig, V. Enkelmann, O. Schmelz, K. Mullen, *Chem. Eur. J.* **2000**, *6*, 1834–1839.
[23] S. M. Draper, D. J. Gregg, E. R. Schofield, W. R. Browne, M. Duati, J. G. Vos, P. Passaniti, *J. Am. Chem. Soc.* **2004**, *126*, 8694–8701; N. T. Lucas, H. M. Zareie, A. M. McDonagh, *ACS Nano* **2007**, *1*, 348–354.
[24] A. Simon, C. Joblin, *J. Phys. Chem. A* **2009**, *113*, 4878–4888 and references therein.
[25] T. Murahashi, M. Fujimoto, M.-a. Oka, Y. Hashimoto, T. Uemura, Y. Tatsumi, Y. Nakao, A. Ikeda, S. Sakaki, H. Kurosawa,

 © 2011 Wiley-VCH Verlag GmbH & Co. KGaA, Weinheim

Science **2006**, *313*, 1104–1107; B. El Hamaoui, L. Zhi, J. Wu, J. Li, N. Lucas, Ž. Tomović, U. Kolb, K. Müllen, *Adv. Funct. Mater.* **2007**, *17*, 1179–1187.
[26] T. Albright, P. Dosa, T. Grossmann, V. Khrustalev, O. Oloba, R. Padilla, R. Paubelle, A. Stanger, T. Timofeeva, K. Vollhardt, *Angew. Chem. Int. Ed.* **2009**, *48*, 9853–9857; H. C. Jahr, M. Nieger, K. H. Dötz, *Chem. Eur. J.* **2005**, *11*, 5333–5342.
[27] F. Nunzi, F. Mercuri, A. Sgamellotti, N. Re, *J. Phys. Chem. B* **2002**, *106*, 10622–10633.
[28] I. Suarez-Martinez, C. P. Ewels, X. Ke, G. Van Tendeloo, S. Thiess, W. Drube, A. Felten, J.-J. Pireaux, J. Ghijsen, C. Bittencourt, *ACS Nano* **2010**, *4*, 1680–1686; K. T. Chan, J. B. Neaton, M. L. Cohen, *Phys. Rev. B* **2008**, *77*.
[29] I. D. Gridnev, *Coord. Chem. Rev.* **2008**, *252*, 1798–1818; J. O. C. Jimenez-Halla, J. Robles, M. Sola, *Organometallics* **2008**, *27*, 5230–5240; T. A. Albright, P. Hofmann, R. Hoffmann, C. P. Lillya, P. A. Dobosh, *J. Am. Chem. Soc.* **1983**, *105*, 3396–3411; H. C. Jahr, M. Nieger, K. H. Dötz, *Chem. Eur. J.* **2005**, *11*, 5333–5342; O. Joistgen, A. Pfletschinger, J. Ciupka, M. Dolg, M. Nieger, G. Schnakenburg, R. Frohlich, O. Kataeva, K. H. Dötz, *Organometallics* **2009**, *28*, 3473–3484; I. D. Gridnev, M. K. C. del Rosario, *Organometallics* **2005**, *24*, 4519–4527; A. Stanger, *Organometallics* **1991**, *10*, 2979–2982.
[30] T. M. Douglas, A. B. Chaplin, A. S. Weller, *Organometallics* **2008**, *27*, 2918–2921.
[31] T. M. Douglas, A. B. Chaplin, A. S. Weller, X. Yang, M. B. Hall, *J. Am. Chem. Soc.* **2009**, *131*, 15440–15456.
[32] N. S. Townsend, A. B. Chaplin, M. A. Naser, A. L. Thompson, N. H. Rees, S. A. Macgregor, A. S. Weller, *Chem. Eur. J.* **2010**, *16*, 8376–8389.
[33] O. Buttler, A. Al-Fawaz, D. L. Kays, J. K. Day, L. L. Ooi, S. Aldridge, *Z. Anorg. Allg. Chem.* **2006**, *632*, 2187–2189.
[34] P. Marcazzan, B. O. Patrick, B. R. James, *Organometallics* **2003**, *22*, 1177–1179.
[35] B. J. Holliday, Y.-M. Jeon, C. A. Mirkin, C. L. Stern, C. D. Incarvito, L. N. Zakharov, R. D. Sommer, A. L. Rheingold, *Organometallics* **2002**, *21*, 5713–5725.
[36] A. Rifat, M. F. Mahon, A. S. Weller, *J. Organomet. Chem.* **2003**, *667*, 1–4.
[37] R. H. Crabtree, C. P. Parnell, *Organometallics* **1984**, *3*, 1727–1731.
[38] M. Reinhold, J. E. McGrady, R. N. Perutz, *J. Am. Chem. Soc.* **2004**, *126*, 5268–5276; T. A. Atesin, T. Li, S. Lachaize, J. J. Garcia, W. D. Jones, *Organometallics* **2008**, *27*, 3811–3817.
[39] M. A. Bennett, M. Bown, D. C. R. Hockless, *Aust. J. Chem.* **2000**, *53*, 507–515.
[40] M. D. Fryzuk, L. Jafarpour, F. M. Kerton, J. B. Love, S. J. Rettig, *Angew. Chem. Int. Ed.* **2000**, *39*, 767–770.
[41] A. Sattler, G. Zhu, G. Parkin, *J. Am. Chem. Soc.* **2009**, *131*, 7828–7838.
[42] P. H. M. Budzelaar, N. N. P. Moonen, R. de Gelder, J. M. M. Smits, A. W. Gal, *Chem. Eur. J.* **2000**, *6*, 2740–2747.
[43] Y. Sevryugina, M. A. Petrukhina, *Eur. J. Inorg. Chem.* **2008**, 219–229.
[44] H. Friebolin, *Basic One- and Two-Dimensional NMR Spectroscopy*, VCH Publishers, New York, **1991**.
[45] A. B. Pangborn, M. A. Giardello, R. H. Grubbs, R. K. Rosen, F. J. Timmers, *Organometallics* **1996**, *15*, 1518–1520.
[46] W. E. Buschmann, J. S. Miller, K. Bowman-James, C. N. Miller, *Inorg. Synth.* **2002**, *33*, 83–85.
[47] J. Cosier, A. M. Glazer, *J. Appl. Crystallogr.* **1986**, *19*, 105–107.
[48] Z. Otwinowski, W. Minor, in: *Processing of X-ray diffraction data collected in oscillation mode*, vol. 276, **1997**, p. 307–326.
[49] G. M. Sheldrick, *Acta Crystallogr.* **2008**, *64*, 112–122.
[50] M. C. Burla, R. Caliandro, M. Camalli, B. Carrozzini, G. L. Cascarano, L. De Caro, C. Giacovazzo, G. Polidori, R. Spagna, *J. Appl. Crystallogr.* **2005**, *38*, 381–388.
[51] A. L. Spek, *J. Appl. Crystallogr.* **2003**, *36*, 7–13.

Received: December 2, 2010
Published Online: February 21, 2011

 © 2011 Wiley-VCH Verlag GmbH & Co. KGaA, Weinheim